Biophysical principles predict fitness landscapes of drug resistance

João V. Rodrigues[a], Shimon Bershtein[b], Annabel Li[c,1], Elena R. Lozovsky[c], Daniel L. Hartl[c,2], and Eugene I. Shakhnovich[a,2]

[a]Department of Chemistry and Chemical Biology, Harvard University, Cambridge, MA 02138; [b]Department of Life Sciences, Ben-Gurion University of the Negev, Beer-Sheva 8410501, Israel; and [c]Department of Organismic and Evolutionary Biology, Harvard University, Cambridge MA 02138

Contributed by Daniel L. Hartl, January 27, 2016 (sent for review November 13, 2015; reviewed by Christopher J. Marx, Dan S. Tawfik, and Claus O. Wilke)

Fitness landscapes of drug resistance constitute powerful tools to elucidate mutational pathways of antibiotic escape. Here, we developed a predictive biophysics-based fitness landscape of trimethoprim (TMP) resistance for *Escherichia coli* dihydrofolate reductase (DHFR). We investigated the activity, binding, folding stability, and intracellular abundance for a complete set of combinatorial DHFR mutants made out of three key resistance mutations and extended this analysis to DHFR originated from *Chlamydia muridarum* and *Listeria grayi*. We found that the acquisition of TMP resistance via decreased drug affinity is limited by a trade-off in catalytic efficiency. Protein stability is concurrently affected by the resistant mutants, which precludes a precise description of fitness from a single molecular trait. Application of the kinetic flux theory provided an accurate model to predict resistance phenotypes (IC_{50}) quantitatively from a unique combination of the in vitro protein molecular properties. Further, we found that a controlled modulation of the GroEL/ES chaperonins and Lon protease levels affects the intracellular steady-state concentration of DHFR in a mutation-specific manner, whereas IC_{50} is changed proportionally, as indeed predicted by the model. This unveils a molecular rationale for the pleiotropic role of the protein quality control machinery on the evolution of antibiotic resistance, which, as we illustrate here, may drastically confound the evolutionary outcome. These results provide a comprehensive quantitative genotype–phenotype map for the essential enzyme that serves as an important target of antibiotic and anticancer therapies.

fitness landscapes | DHFR | drug resistance | protein stability | molten globule

Predictive models of antibiotic resistance are key to developing novel antibacterial treatments (1–6). Besides its practical importance, antibiotic escape presents a tractable general model of adaptive evolutionary dynamics that can provide insights into fundamental questions in evolution, such as the reproducibility and predictability of evolutionary trajectories (4, 7, 8) as well as the importance of epistasis and pleiotropy (5, 7, 9, 10).

Experimental evolution studies of evolution of antibiotic resistance showed that in many cases resistance-conferring mutations arose both in target and off-pathway genes (5, 11). However, mutations conferring resistance against trimethoprim (TMP) were largely limited to the target gene, namely the ORF and upstream region of *folA,* the gene encoding dihydrofolate reductase (DHFR) (1, 5, 11). DHFR is an essential core metabolic enzyme that converts dihydrofolate to tetrahydrofolate—a main source of carbon atoms in several key pathways. The rare occurrence of off-target adaptive mutations makes DHFR an attractive model to study the fitness landscape of antibiotic resistance. In a recent study (2) strains carrying various combinations of TMP resistance-conferring mutations in *folA* were incorporated onto the *Escherichia coli* chromosome (12, 13) and their fitness (growth rate) was determined, providing the fitness landscape for the chosen set of variants. The analysis in ref. 2 demonstrated the complexity of the fitness landscape of TMP resistance featuring strong epistasis, although the underlying molecular mechanisms giving rise to the epistatic interactions between DHFR mutations remained unknown. Further, the genotype–phenotype link was determined only for a selected set of genetic variants and only under conditions (temperature and concentration of antibiotic) at which fitness was determined. It is an ongoing challenge to predict fitness landscape for a broad set of conditions and genetic variations that might arise in the process of evolutionary dynamics of adaptation in vivo and in the laboratory. To that end we need to close the genotype–phenotype gap for the target protein by establishing the fundamental physical–chemical link between the molecular effects of mutations and their fitness effects.

Here we address these challenges using DHFR as a model system. Among mutations identified in the evolutionary experiment under sustained selection toward TMP resistance (1), P21L, A26T, L28R, and their combinations constitute an interesting set that recurrently appeared in two out of five independent evolution experiments, and their order of fixation in both cases was similar. These mutated residues cluster within a short region of eight residues in the DHFR protein that comprises a flexible Met-20 loop (residues 9–24) and an α-helix (residues 25–35) that establishes contacts with bound dihydrofolate substrate (Fig. 1*A*).

We purified all possible combinations of these three key DHFR mutations that confer TMP resistance (depicted in Fig. 1*B*) and determined their biophysical properties (activity, stability, and binding affinity to TMP). We transformed *E. coli* with pFLAG plasmids expressing WT and mutant *E. coli* DHFR gene constructs and measured the intracellular DHFR abundance and determined fitness (growth rates) of each transformed variant in a broad range of concentrations of TMP. We also extended the mutational analysis to DHFR originated in *Chlamydia muridarum* and *Listeria grayi* by creating the

Significance

Development of predictive models of antibiotic resistance is challenging due to a lack of understanding of the relationship between molecular and fitness effects of mutations (the genotype–phenotype gap). Here we close the genotype–phenotype gap for an essential enzyme, dihydrofolate reductase (DHFR), which is an important target of the common antibiotic trimethoprim. We show that IC_{50} of trimethoprim resistance of *Escherichia coli* can be predicted, with high accuracy, from a unique combination of molecular properties of stepwise-resistant DHFR variants. These results show that the challenge to predict de novo evolutionary dynamics of antibiotic resistance lies in the need for accurate prediction of the effects of mutations on the molecular properties of target enzymes.

Author contributions: D.L.H. and E.I.S. designed research; J.V.R. and S.B. performed research; S.B., A.L., and E.R.L. contributed new reagents/analytic tools; J.V.R., S.B., and D.L.H. analyzed data; and J.V.R. and E.I.S. wrote the paper.

Reviewers: C.J.M., University of Idaho; D.S.T., Weizmann Institute of Science; and C.O.W., The University of Texas at Austin.

The authors declare no conflict of interest.

[1]Present address: Warp Drive Bio, LLC., Cambridge, MA 02139.

[2]To whom correspondence may be addressed. Email: dhartl@oeb.harvard.edu or shakhnovich@chemistry.harvard.edu.

This article contains supporting information online at www.pnas.org/lookup/suppl/doi:10.1073/pnas.1601441113/-/DCSupplemental.

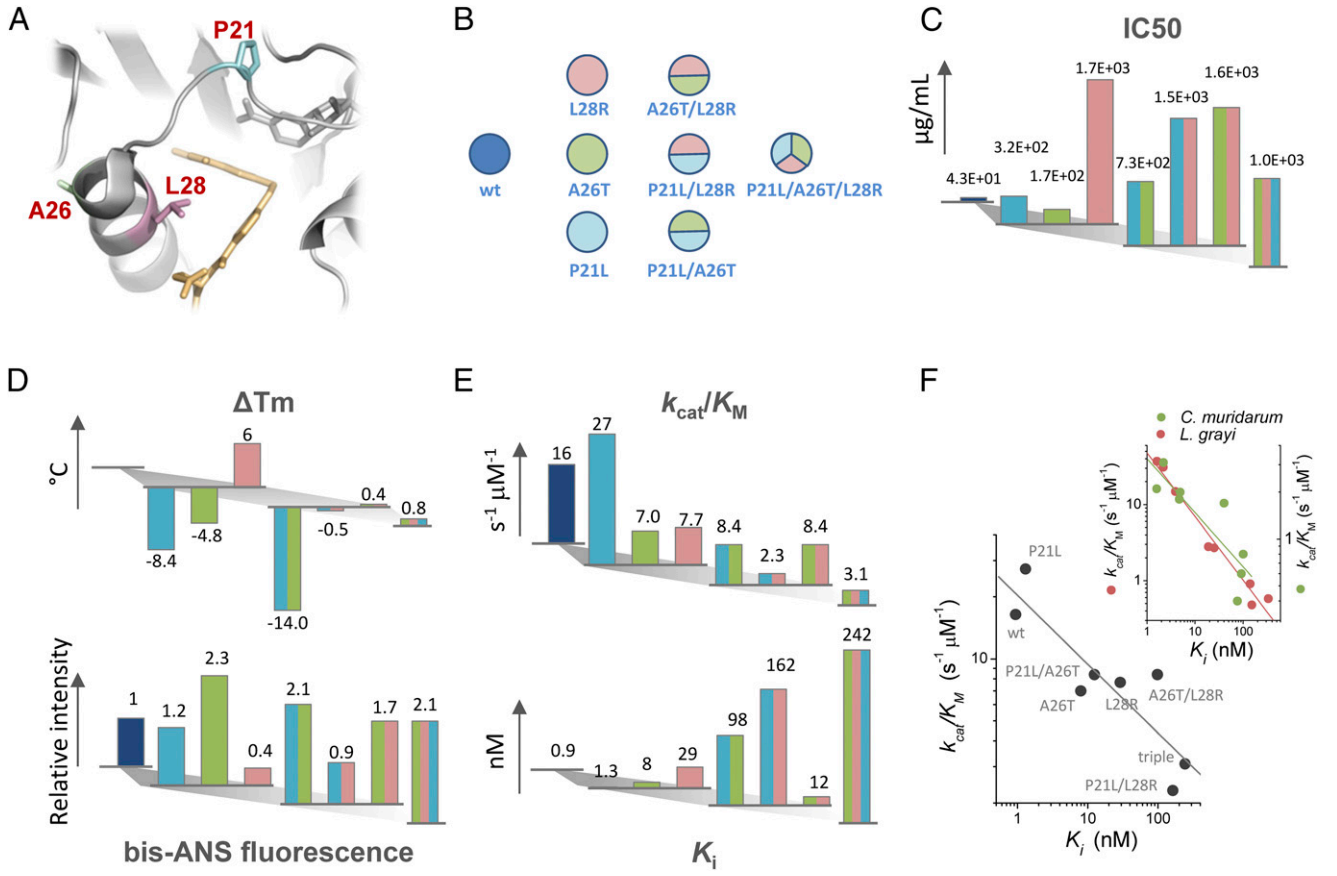

Fig. 1. DHFR mutations associated with TMP resistance and mapping of phenotypic and molecular effects in a combinatorially complete set of mutations. (*A*) Resistance-conferring mutations in DHFR are found close to binding pocket of dihydrofolate (in yellow). (*B*) Color-code scheme of all possible combination made out of the three mutations studied in this work. (*C*) IC_{50} values determined for *E. coli* transformed with pFLAG plasmid harboring different DHFR mutants. (*D*) Stability data measured for different DHFR mutants. (*Top*) ΔT_m values were determined from thermal denaturation experiments monitored by the change in tryptophan fluorescence upon unfolding. (*Bottom*) bis-ANS fluorescence upon binding to different DHFR mutants measured after incubation at 37 °C for 5 min. (*E*) Catalytic parameters determined for all DHFR mutants. (*Top*) Catalytic efficiency measured at 25 °C from full progress reaction curves. (*Bottom*) TMP inhibition constants (K_i) determined at 25 °C. (*F*) Catalytic efficiency trades-off with increase in K_i. (*Inset*) A similar trade-off observed for orthologous DHFR mutants from *L. grayi* and *C. muridarum*.

corresponding set of mutations in the matching positions of the orthologous sequences.

We found that TMP resistance mutations affect multiple molecular properties of DHFR so that no single molecular trait is predictive of fitness. However, flux dynamics theory (14, 15) predicts, and experiments demonstrate, that fitness and IC_{50} for TMP can be accurately predicted when the combined effect of mutations that simultaneously change the abundance, activity, and TMP binding affinity of mutant DHFR are taken into account. Further, using the earlier established relationship (13) between DHFR abundance (cellular property) and population of the molten globule state (molecular property of DHFR), we show that the fitness landscape of DHFR mutations can be derived from the molecular properties of DHFR alone. This multiscale analysis provides an example of a predictive quantitative biophysical fitness landscape for an essential enzyme.

Results

Fitness Landscape of TMP Resistance. Growth measurements were done in the absence of inducer (isopropyl β-D-1-thiogalactopyranoside, IPTG) because leaky expression from plasmid was sufficient to confer high levels of TMP resistance (~100-fold over nontransformed cells), and yet the resistance was relatively modest, so inhibition of growth could be observed. To quantify growth at each TMP concentration we integrated the area under the growth curve (optical density vs. time) as described in ref. 2 and for each variant determined the level of TMP resistance by measuring IC_{50} (*SI Methods*). Expectedly, all mutations confer increased resistance to TMP over WT DHFR (Fig. 1*C* and Dataset S1), consistent with earlier results where the same mutations were introduced into the *E. coli* chromosome (2). Among single mutants, the L28R variant exhibits by far the highest resistance. Introduction of another mutation on the L28R background, either P21L or A26T, does not change IC_{50} significantly. On the contrary, the resistance of the double mutant P21L/A26T is best interpreted as arising from an additive effect of the combined contributions of each mutation. Although the triple mutant P21L/A26T/L28R emerged in laboratory evolution as the winning allele at highest concentration of TMP (1), it is the most drug-sensitive among all L28R-containing variants.

To provide a mechanistic insight into the phenotypic differences between different DHFR variants, all protein variants were purified to homogeneity and characterized in vitro for their stability and catalytic properties.

Stability of DHFR Mutants. All purified DHFR mutants were determined to be monomers by size-exclusion chromatography, with no evidence for a significant amount of higher oligomeric states (Fig. S1). Thermal denaturation experiments, which allow assessing differences in protein stability, were performed for each protein variant (Fig. S1 and *Methods*). Mutational changes

in protein folding stability characterized by the difference in the midpoint denaturation transition temperature with respect to WT (ΔT_m) are shown in Fig. 1*D*, *Top*. It is clear that P21L and A26T mutations are destabilizing, in contrast to the stabilizing mutation L28R, which shows an increase in T_m of 6 °C above WT DHFR. The significant lower stability observed for the double mutant P21L/A26T (−14 °C) is probably the result of the additive contribution of each destabilizing mutation. Interestingly, the L28R mutation cancels out the destabilization brought by P21L and A26T, restoring the T_m of the double and triple mutants to WT values. In addition to thermal stability, the propensity of DHFR mutants to form molten-globule intermediates was measured using the fluorescent dye bis-ANS as a reporter (13, 16) (Fig. 1*D*, *Bottom*). Increased fluorescence indicates an increased exposure of protein hydrophobic patches to which the dye binds, which correlates with molten-globule content (17). High bis-ANS fluorescence at 37 °C is observed in all DHFR variants that have the A26T mutation, suggesting a particular effect of this mutation on the increase of the subpopulation of molten-globule–like conformations. As with thermal stability, the single L28R mutant also shows improved compactness, inferred from its low bis-ANS binding properties; however, in double and triple mutants, L28R does not compensate the deleterious effects caused by A26T.

Escaping Drug Inhibition Involves Catalytic Efficiency Trade-Off. Owing to the proximity of all three mutated residues to the active site, it is expected that mutations will significantly affect the catalytic activity of the protein. The catalytic activity (k_{cat}/K_m) was determined from the analysis of full-progress reaction curves, as described previously (18); k_{cat}/K_m has the physical meaning of a second-order rate constant for the reaction between DHFR and dihydrofolate (under nonsaturating concentrations of dihydrofolate and saturating concentration of the cofactor NADPH). Fig. 1*E*, *Top* shows a progressive decrease in k_{cat}/K_m as more mutations are successively added to the protein. This drop in efficiency is caused mainly by the drop in the reaction turnover (k_{cat}), because K_m for dihydrofolate also decreases (Fig. S2). To investigate whether binding of TMP to the active site of DHFR is affected by mutations, we measured the kinetic inhibition constant (K_i) for each variant. This parameter was determined by measuring the drop in DHFR catalytic activity at increasing concentrations of TMP, using fixed dihydrofolate concentrations (see details in *SI Methods*). In contrast to what was observed for catalytic efficiency, there is a dramatic increase in K_i as mutations accumulate, reaching a maximum at the triple mutant. In fact, there is a noticeable anticorrelation between catalytic efficiency and K_i, indicating a clear trade-off between catalytic efficiency and increased drug resistance (Fig. 1*F*).

Fitness Landscapes of Orthologous Transformations. To get a broader view of the biophysical nature of the fitness landscape of antibiotic resistance we also transformed *E. coli* with pFLAG plasmids expressing DHFR proteins from two mesophilic bacteria, *C. muridarum* and *L. grayi*, sharing 26% and 36% sequence identity with *E. coli* DHFR, respectively, and carrying all combinations of the three key mutations in the loci corresponding to the three escape mutations in *E. coli* DHFR that we study here (see sequence alignment in Fig. S3). Similarly to *E. coli* DHFR, we purified all variants of the mutant orthologs from *C. muridarum* and *L. grayi*, characterized their biophysical properties, and compared them with *E. coli* DHFR mutants (Figs. S2 and S4). We observed a similar trade-off between catalytic activity and TMP binding (Fig. 1*F*, *Inset*). The following quantitative analysis of the biophysical fitness landscape includes all strains, that is, transformed with *E. coli* variants and variants of orthologous DHFR from *C. muridarum* and *L. grayi*. Using DHFRs from two additional sources allowed us to significantly extend the dynamic range of biophysical parameters to provide a comprehensive biophysical mapping of the fitness landscape.

Intracellular Protein Abundances Are Inversely Correlated with bis-ANS Binding. The effect of mutations on the total amount of intracellular functional protein (13) can have a significant impact on its evolutionary fate; the benefit of a mutation in conferring high drug resistance to a protein can be completely negated if such a mutation dramatically decreases protein abundance in the cell. Therefore, we developed a fluorescence-based method to quantify intracellular DHFR levels by measuring the total enzymatic activity in cell lysates (see details in *SI Methods*). This assay detects only the fraction of protein that is functional and therefore is biologically more relevant than standard approaches based on Western blotting. This approach was used to determine the concentration of chromosomally expressed DHFR from the parent MG1655 strain, which yielded ∼90 copies per cell in accord with the earlier estimate (19), whereas the noninduced overexpression from pFLAG plasmid produced 300-fold greater number of copies of protein (∼24,000 molecules per cell for WT DHFR). Fig. 2*A* shows the intracellular abundances of *E. coli* DHFR variants expressed from the plasmid under growth conditions identical to those used in the IC_{50} measurements. These values (which were normalized to plasmid-expressed *E. coli* WT DHFR abundance) vary from 0.4- (triple mutant) to 2.8-fold (P21L/L28R double mutant). Similar measurements performed for the orthologous DHFR from *C. muridarum* and *L. grayi* indicate that these variants are expressed at much lower levels (Fig. S5 and Dataset S2). Indeed, we observe a strong inverse correlation between abundance and fraction of molten-globule intermediate state assessed by bis-ANS binding (Fig. 2*B*); no significant correlation is observed between abundance and ΔT_m (Fig. S5). In a cellular environment, the DHFR steady-state concentration is governed by the competing action of chaperonins GroEL/ES and protease Lon, which bind molten-globule intermediates of DHFR. Therefore, mutations that change the folding equilibrium toward the formation of molten-globule state shift the protein turnover balance toward degradation, affecting its total abundance. Specifically, the abundance of a DHFR mutant variant in an active cellular milieu is inversely proportional to its in vitro ANS fluorescence, which serves as a readout for fraction of proteins in molten-globule state. This relation was previously predicted (and experimentally verified) in the model of active cytoplasm proposed in our laboratory (13).

Establishing a Quantitative Genotype-to-Phenotype Relationship for DHFR in *E. coli*. The results presented so far illustrate both the broad impact of mutations on multiple molecular traits (catalytic efficiency, K_i, and protein stability). This renders the fitness landscape in terms of molecular properties highly multidimensional, making its description from molecular parameters quite challenging. To overcome this, we sought to develop a simple model that allows a quantitative prediction of the impact of a given physical property at the phenotype level. We have recently studied diverse orthologous replacements of bacterial DHFR in *E. coli* and demonstrated that fitness, as assessed by cell growth, depends on the flux through DHFR (20) and can be described using the following equation derived in ref. 14:

$$fitness \sim flux = a\frac{V_{dhfr}}{(B+V_{dhfr})}, \quad [1]$$

where V_{dhfr} is the rate at which dihydrofolate is converted to tetrahydrofolate, B is a constant related to the effect of all other proteins in the enzymatic chain (14, 15), and a denotes maximal fitness at highest flux. Taking into account the competitive mechanism of

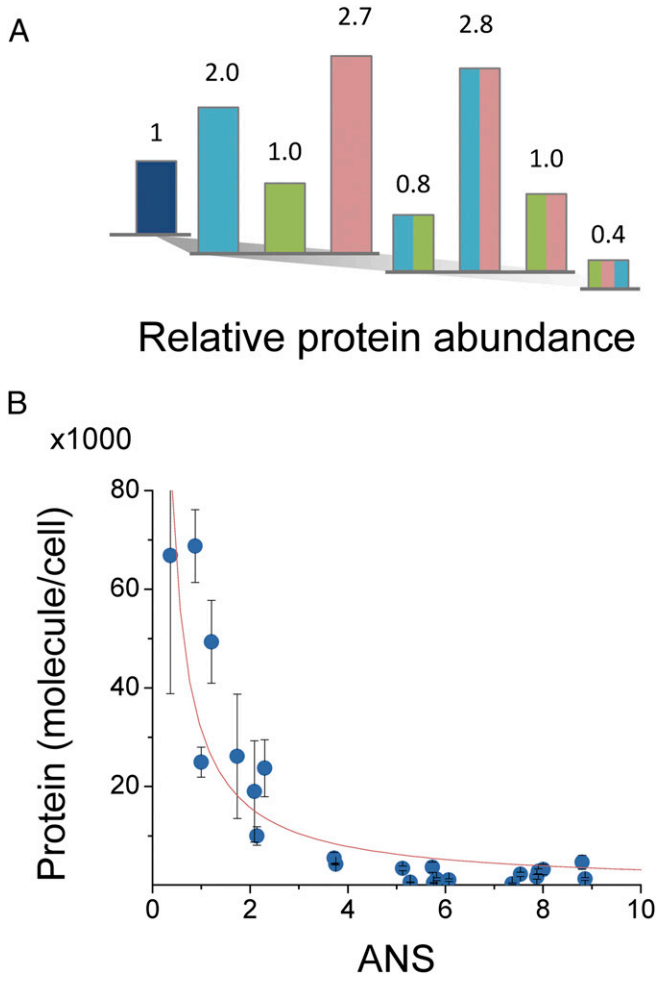

Fig. 2. Mutations associated with TMP resistance affect the intracellular abundance of DHFR. (*A*) Intracellular abundance of *E. coli* DHFR mutants expressed from pFLAG plasmid in the absence of inducer (color scheme as in Fig. 1*B*). Abundance was determined from total catalytic activity measurements in cell lysates prepared from cultures of different mutants grown at 37 °C in M9 minimal media. Values are normalized to WT DHFR expressed from plasmid at the same conditions. (*B*) Protein abundance is inversely correlated with propensity to form molten-globule intermediates, as assessed by bis-ANS fluorescence. The represented data (mean ± SEM) were obtained from abundance measurements of *E. coli* DHFR mutants and orthologous DHFRs from *L. grayi* and *C. muridarum* including the cognate TMP-resistance mutations. The fit that is shown was obtained using the equation $y = A/(\gamma \cdot ANS)$, where $A = 4.7 \times 10^5$ molecules/cell and $\gamma = 1.5$.

inhibition by TMP, and considering that DHFR can be treated as a one-substrate enzyme [due to saturating concentrations of intracellular NADPH (21)], V_{dhfr} can be expressed by a general Michaelis–Menten-like curve:

$$V_{dhfr} = \frac{k_{\mathrm{cat}} \cdot [DHFR] \cdot [FH_2]}{K_{\mathrm{m}} \cdot \left(1 + \frac{\alpha \cdot [TMP]_{medium}}{K_i}\right) + [FH_2]}, \qquad [2]$$

where $[DHFR]$ and $[FH_2]$ are the intracellular concentrations of DHFR and dihydrofolate, respectively, and $[TMP]_{medium}$ is the concentration of TMP in the growth medium. The parameter α is the ratio between the intracellular TMP concentration and that in the growth medium; below we explain how this parameter is determined. Our basic assumptions in this model are that (*i*) the enzymatic reaction occurs at conditions far from substrate saturation and (*ii*) the intracellular concentration of dihydrofolate (FH_2) is constant so that the reaction becomes pseudo–first-order with respect to DHFR intracellular concentration:

$$V_{dhfr} \approx k_{app} \cdot [DHFR] \cdot \frac{1}{\left(1 + \frac{\alpha \cdot [TMP]_{medium}}{K_i}\right)},$$

when [3]

$$K_{\mathrm{m}}\left(1 + \frac{\alpha \cdot [TMP]_{medium}}{K_{\mathrm{i}}}\right) \gg [FH_2],$$

where

$$k_{app} = \frac{k_{\mathrm{cat}}}{K_{\mathrm{m}}} \cdot [FH_2]_{fixed}.$$

To simplify the analysis, we define a normalized reaction rate, V^{norm}, by dividing the left side of Eq. **3** by $[FH_2]$ and by the catalytic efficiency ($k_{\mathrm{cat}}/K_{\mathrm{m}}$) of WT *E. coli* DHFR:

$$V_{dhfr}^{norm} = \frac{\frac{k_{\mathrm{cat}}^{mut}}{K_{\mathrm{m}}^{mut}}}{\frac{k_{\mathrm{cat}}^{EcoliWT}}{K_{\mathrm{m}}^{EcoliWT}}} \cdot [DHFR]^{mut} \cdot \frac{1}{\left(1 + \frac{\alpha \cdot [TMP]_{medium}}{K_{\mathrm{i}}^{mut}}\right)}, \qquad [4]$$

where $[k_{\mathrm{cat}}/K_{\mathrm{m}}]^{mut}$, $[DHFR]^{mut}$, and K_{i}^{mut} are the catalytic efficiency, intracellular concentration, and inhibition constant of a particular DHFR mutant. Because all variables are known from in vitro protein characterization and cellular abundance measurements, V^{norm} can be directly estimated for every mutant at any given TMP concentration at which a growth measurement is performed. This allows us to explore the genotype–phenotype link between the DHFR normalized reaction rate and fitness. Such dependence is depicted in Fig. 3*A*, which shows the data for a total of 24 DHFR variants (including *E. coli*, *L. grayi*, and *C. muridarum*) obtained at 12 different TMP concentrations (Dataset S3). It should be noted that the decrease in DHFR activity due to TMP inhibition increases the control coefficient of the DHFR-catalyzed reaction toward 1.0 so that the flux of the entire pathway becomes largely dependent on that reaction and growth drops proportionally.

We determined the TMP penetration ratio parameter α by fitting the present measurements of fitness in the presence of TMP shown in Fig. 3*A* to the fitness data from previous studies obtained by variation of DHFR properties without TMP [down-regulation of DHFR expression using IPTG-controllable promoter (13) and chromosomal orthologous replacements of DHFR (20)]. The best superposition of data is achieved at $\alpha = 0.1$, which is very close to the earlier direct measurements of fraction of TMP penetrating into bacterial cytoplasm (22) (see *Supporting Information* and Fig. S6 for details). There is a remarkable superimposition of all data, in particular around the steep drop in fitness. Similar, albeit a bit noisier, results are obtained if fitness is defined as the maximal growth rate instead of using the integral of the growth curve (Fig. S7). A set of points obtained for untransformed parent *E. coli* strain MG1655, expressing solely its WT chromosomal DHFR, grown at different TMP concentrations shows a good superimposition as well [with slight deviation at higher fitness probably due to activation of the DHFR promoter through a feedback loop (23, 24)]. Also included for comparison are the data points obtained in previous studies using chromosomal orthologous DHFR replacements (20) and an IPTG-inducible promoter-controlled chromosomal DHFR expression system (13). Fitting the data points with Eq. **1** resulted in an excellent quantitative prediction of fitness, in agreement with recent work (20). The parameter *B* resulting from the nonlinear fit of Eq. **1** to all data

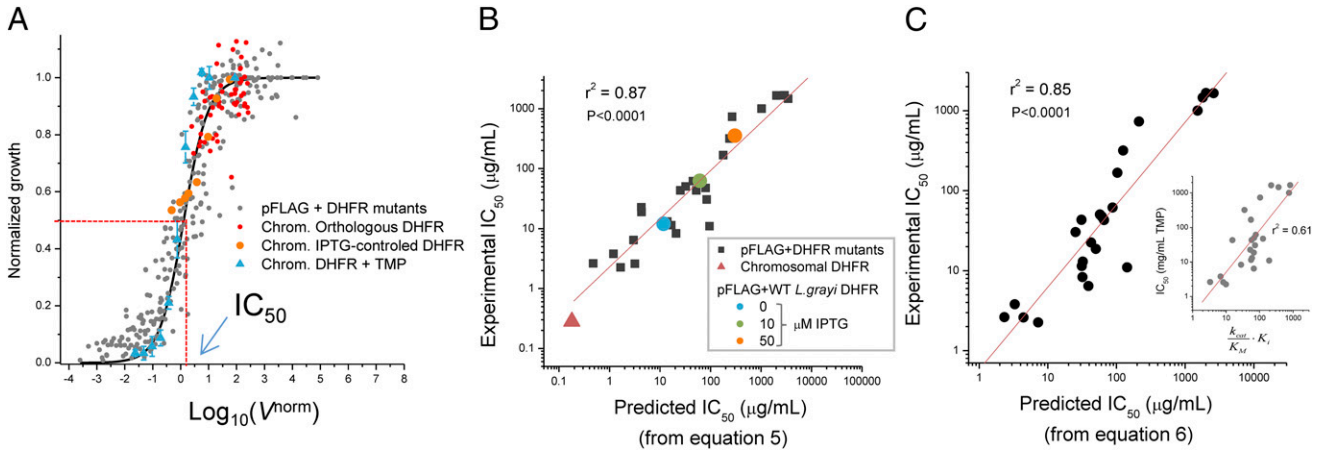

Fig. 3. Prediction of IC_{50} from molecular parameters. (*A*) Normalized rate of DHFR reaction(V^{norm}) determines fitness in *E. coli*. Growth measurements were performed at 37 °C in M9 minimal media and under varying concentrations of TMP. The V^{norm} values were computed at any given TMP concentration using Eq. **4**, in which α was set to 0.1, and with input from experimentally determined molecular quantities (protein abundance and catalytic constants) for each DHFR mutant. The results shown include data from TMP inhibition determined for all *E. coli*, *L. grayi*, and *C. muridarum* DHFR mutants expressed from pFLAG plasmid (gray) and nontransformed *E. coli* MG1655 strain expressing solely its endogenous chromosomal DHFR (blue). The solid line represents the best fit of the data using Eq. **1** with $a = 1$, and from which B was determined from nonlinear regression (1.3 ± 0.1 SE). Also shown for comparison are the fitness data obtained in previous works where orthologous DHFRs have been incorporated in *E. coli* chromosome (20) and where chromosomal DHFR was under IPTG-controlled expression (13) (red and orange points, respectively). (*B*) Comparison of experimental vs. predicted IC_{50} for TMP in strains expressing DHFR mutants from pFLAG. Predicted IC_{50} were calculated from Eq. **5** using estimates of cellular DHFR abundance and catalytic parameters. Increasing the pFLAG-based expression of a particular mutant DHFR by means of adding IPTG results in corresponding increase in IC_{50} as predicted from Eq. **5**. Data obtained for parent strain MG1655 *E. coli* expressing only its chromosomal DHFR are shown. (*C*) Prediction of fitness from protein biophysics. IC_{50} was predicted using Eq. **6**, in which the protein abundance term in Eq. **5** was replaced by 1/ANS from the reciprocal relationship shown in Fig. 2. (*Inset*) The decrease in the correlation coefficient if the protein abundance term, or its predictor (1/ANS), is omitted in the equation.

points was found to be $B = 1.3 \pm 0.1$, whereas the average of B values determined from independent fits of the growth data obtained for each individual mutant DHFR strain at different concentrations of TMP was 1.7 ± 0.4 (mean ± SE). The flux model therefore allows quantitative prediction of drug resistance and fitness (expressed as IC_{50}) from molecular parameters of DHFR. The observed relationship in Fig. 3*A* holds in a broad range of parameters, especially with the absolute intracellular DHFR concentration ranging from ∼90 copies per cell (MG1655 strain, chromosomal expression) to ∼70,000 copies per cell (*E. coli* double mutant P21L/L28R, pFLAG expression), the catalytic efficiency (k_{cat}/K_m) values ranging from 0.1 to 37 $\mu M^{-1}\cdot s^{-1}$, and the inhibition constant K_i ranging from 1 to 330 nM (see Table S1 for the full list).

Predicting IC_{50} from DHFR Biophysics. It is clear from Eq. **1** that fitness is halved when V^{norm} is equal to the constant B. Therefore, the left-hand side of Eq. **4** can be set equal to B when the TMP concentration corresponds to IC_{50}. From the resulting equation it is possible to directly compute TMP IC_{50} for a given DHFR mutant:

$$IC_{50}^{mut} = \frac{1}{\alpha B}\cdot\frac{\frac{k_{cat}^{mut}}{K_m^{mut}}}{\frac{k_{cat}^{EcoliWT}}{K_m^{EcoliWT}}}\cdot[DHFR]^{mut}\cdot K_i^{mut} - \frac{1}{\alpha}\cdot K_i^{mut}. \quad [5]$$

Fig. 3*B* shows a clear linear relationship between measured IC_{50} and the prediction from Eq. **5** (slope = 0.80, $r^2 = 0.87$, $P < 0.001$). Such high correlation is achieved when all three factors—abundance, catalytic activity, and TMP binding affinity—are taken into account. The predictive power is greatly diminished if any of the variables in Eq. **5** is dropped (Fig. S8). For example, binding affinity K_i or catalytic activity k_{cat}/K_m alone are poor predictors of antibiotic resistance IC_{50} ($r^2 = 0.13$ and 0.08, respectively). Statistically significant yet weaker predictions of IC_{50} can be obtained using solely the product $k_{cat}/K_m \times K_i$ ($r^2 = 0.61$, $P < 0.001$) or protein abundance alone ($r^2 = 0.625$, $P < 0.001$), yet only the full combination of all three biophysical parameters as given by Eq. **5** can provide highly accurate predictions. This result demonstrates that the model chosen to predict fitness is quite robust, even though it was based on several simplifying assumptions. One important prediction from Eq. **5** is that the IC_{50} of any given mutant should vary proportionally to intracellular concentration of DHFR when other molecular parameters remain unchanged. This prediction was tested by increasing the DHFR expression from the plasmid using different amounts of inducer IPTG and is highlighted in Fig. 3*B* for WT *L. grayi*. Similar experiments were performed with a set of mutants from *L. grayi* and *C. muridarum* (Fig. S8), but not for *E. coli* DHFR WT and mutants because overexpression of *E. coli* DHFR is toxic to *E. coli* (25).

Our analysis based on Eq. **5** indicates that both molecular (k_{cat}/K_m and K_i) and cellular (protein abundance) properties of DHFR need to be established for accurate prediction of IC_{50}. However, the relationship existing between a particular molecular trait of DHFR, namely its in vitro ANS fluorescence and intracellular abundance, as established in ref. 13 and confirmed here (Fig. 2*B*), allows prediction of IC_{50} solely from the molecular properties of DHFR by replacing the term [*DHFR*] in Eq. **5** by 1/*ANS*:

$$IC_{50}^{mut} = \frac{1}{\alpha B}\cdot\frac{\frac{k_{cat}^{mut}}{K_m^{mut}}}{\frac{k_{cat}^{EcoliWT}}{K_m^{EcoliWT}}}\cdot\frac{A}{\gamma ANS}\cdot K_i^{mut} - \frac{1}{\alpha}\cdot K_i^{mut}, \quad [6]$$

where A and γ are parameters derived from the fit shown in Fig. 2*B*. Indeed Fig. 3*C* shows that this approximation results in a fairly good prediction of IC_{50} (slope = 1.0, $r^2 = 0.86$, $P < 0.001$). This result shows that fitness in the presence of antibiotic can be predicted exclusively from biophysical parameters of arising DHFR mutants, given that growth conditions (e.g., concentration of the inducer) remain the same.

Epistasis. We can evaluate the degree of epistasis in the effect of mutations on all measured molecular, cellular, and fitness traits. We use the definition of epistasis introduced in ref. 10 as

$$\varepsilon_{AB} = \log\frac{W_{AB}W_0}{W_A W_B} = \log\frac{W_{AB}}{W_0} - \log\frac{W_A}{W_0} - \log\frac{W_B}{W_0}, \qquad [7]$$

where W_0, W_A, W_B, and W_{AB} are values of a trait for WT, mutant A, mutant B, and double mutant AB alleles, respectively. Here we consider epistasis in the effect of mutation on all molecular traits, abundance (cellular trait), and fitness represented by IC_{50} values for each mutant. The results presented in Table 1 for *E. coli* mutants show predominantly negative epistasis with some notable exceptions such as k_{cat}/K_m for L28R/A26T and K_i for L28R/P21L, which probably reflects the fact that L28R is a stabilizing mutation. All mutations show negative epistasis in IC_{50}, due to the trade-offs that reflect pleiotropic effects of mutations on molecular traits of DHFR.

Protein Quality Control Affects the Fitness Landscape. In the earlier work (13) we established the role of protein quality control (PQC) machinery, in particular GroEL chaperonins and Lon protease, in rescuing fitness of *E. coli* DHFR deleterious mutants and orthologous DHFR replacements from different bacteria. We asked how PQC would act on TMP-resistant mutants and thus affect their fitness under antibiotic selection pressure. To that end, we measured IC_{50} and protein abundances for all *E.coli* and orthologous DHFR mutants on the background of GroEL overexpression (GroEL+; see details in *SI Methods* and ref. 13) or Lon knockout (Δ*lon*). Fig. 4*A* shows the different effects of GroEL+ and Δ*lon* on IC_{50} determined for DHFR mutants from *E. coli*, *L. grayi*, and *C. muridarum*. With some exceptions, GroEL+ and Δ*lon* have a neutral or even deleterious effect on *E. coli* DHFR mutants. Notably, the *E. coli* DHFR triple mutant benefits most from GroEL+ background and especially Δ*lon*, the latter resulting in a doubling of its IC_{50}. Apparently, the fitness landscape on the Δ*lon* background is different from the one shown in Fig. 1*C*, because the triple mutant seems to be most fit at high concentration of TMP. The effects of GroEL+ and Δ*lon* on DHFR from *L. grayi* and *C. muridarum* are more pronounced, especially for double and triple mutants, increasing in some cases IC_{50} by one order of magnitude. Remarkably, the magnitude of the effects observed for GroEL+ and Δ*lon* correlate quite well with bis-ANS properties of the DHFR mutants (Fig. S9), in agreement with previous results showing that both components of PQC affect DHFR molten-globule–like intermediates (13).

Fig. 4*B* shows that changes in IC_{50} caused by GroEL overexpression or Lon deletion can be directly attributed to their impact on protein abundance, as expected from Eq. **5**.

Altogether, these results show how the fitness landscape can drastically change by the action of PQC through its effect on the steady-state concentration of protein. Again, the importance of protein biophysical properties is highlighted, in particular ANS binding, because these properties determine, at least in part, how specific DHFR mutants may be rescued/degraded by cellular chaperones and proteases.

Deconvolution of Fitness into Microlandscapes Shows Strong Epistasis. Analysis of the fitness landscape of a complete combinatorial set of mutations, as in this work, is particularly helpful in determining which trajectories are accessible in evolutionary dynamics. This can be regarded as a macroscopic integrated map, which is built upon multiple microscopic landscapes, one for each molecular trait. From this perspective, Eq. **5** is particularly useful because it allows dissection of fitness into microlandscapes, as shown in Fig. 5, where the contribution of each property into fitness effect is mapped for every mutation in a quantitative way. Such analysis helps to highlight which molecular features mostly affect IC_{50}, improving our understanding of what molecular factors shape evolution at different stages of selection. For instance, it becomes obvious that changes in the ability to escape drug (K_i) are the key determinants of the drug resistance, especially at later stages of evolution (double and triple mutants), because variations in protein abundance are comparably smaller (Fig. 5 *B* and *C*). Nevertheless, because the effective catalysis parameter ($k_{cat}/K_m \times K_i$) is not very high in single mutants (except L28R), compared with double and triple mutants, one can expect that other competing mutations occurring genomewide that might result in a significant increase in DHFR abundance could give a selective advantage over single mutations in the active site of DHFR. Interestingly, in the evolutionary experiment against TMP, mutations in the DHFR promoter region were frequently fixed first, resulting in a >10-fold increase in IC_{50} (1). In particular, the mutation –35C→T in the DHFR promoter has been shown to be associated with increased production of *folA* gene product (26). However, mutants with the highest $k_{cat}/K_m \times K_i$ such as A26T/L28R and the triple mutant should benefit more than P21L/L28R or P21L/A26T from any increase in protein abundance that may be caused by a pleiotropic effect of mutations occurring outside of *folA* locus. Inactivation or down-regulation of Lon protease, which effect is shown in Fig. 4, may constitute one such mechanism, and, in fact, has been observed recently during the evolution of strains with orthologous replacements of DHFR (20) and in the evolution of antibiotic resistance (5, 27).

Discussion

The metaphor of fitness landscape is widely used to highlight certain aspects of the genotype–phenotype relationship. It is either postulated a priori (28) or presents a mapping of known genetic variants to fitness (2, 4). However, the most detailed form of a fitness landscape, where each possible genetic variant is mapped to fitness, would be prohibitively complex. An alternative way to provide a tractable and predictive fitness landscape would be to use an intermediate phenotype to map fitness onto molecular properties of the target enzyme (13, 20, 29, 30). This approach runs the risk that important biology could be lost upon projection of fitness onto a limited set of molecular properties. In this work we showed that mapping fitness to molecular properties of DHFR provides an accurate and predictive fitness landscape that establishes the quantitative genotype–phenotype

Table 1. Prevalence of negative epistasis in the effect of mutations on molecular and fitness traits of *E. coli* DHFR

DHFR mutant	IC50	k_{cat}/K_M	K_i	$k_{cat}/K_M \times K_i$	T_m	ANS	abundance	$k_{cat}/K_M \times K_i \times$ abundance
A26T/L28R	–0.59	0.41	–0.42	–0.02	0.00	–0.27	–0.43	–0.37
P21L/L28R	–0.92	–0.75	0.59	–0.07	0.03	–0.27	–0.29	–0.42
P21L/A26T	–0.23	–0.14	0.02	–0.06	–0.01	0.12	–0.40	–0.68
P21L/A26T/L28R	–1.67	–0.25	–0.19	–0.36	0.07	–0.28	–1.13	–1.48

positive
neutral*
negative

*The threshold of neutrality is defined as 0.1.

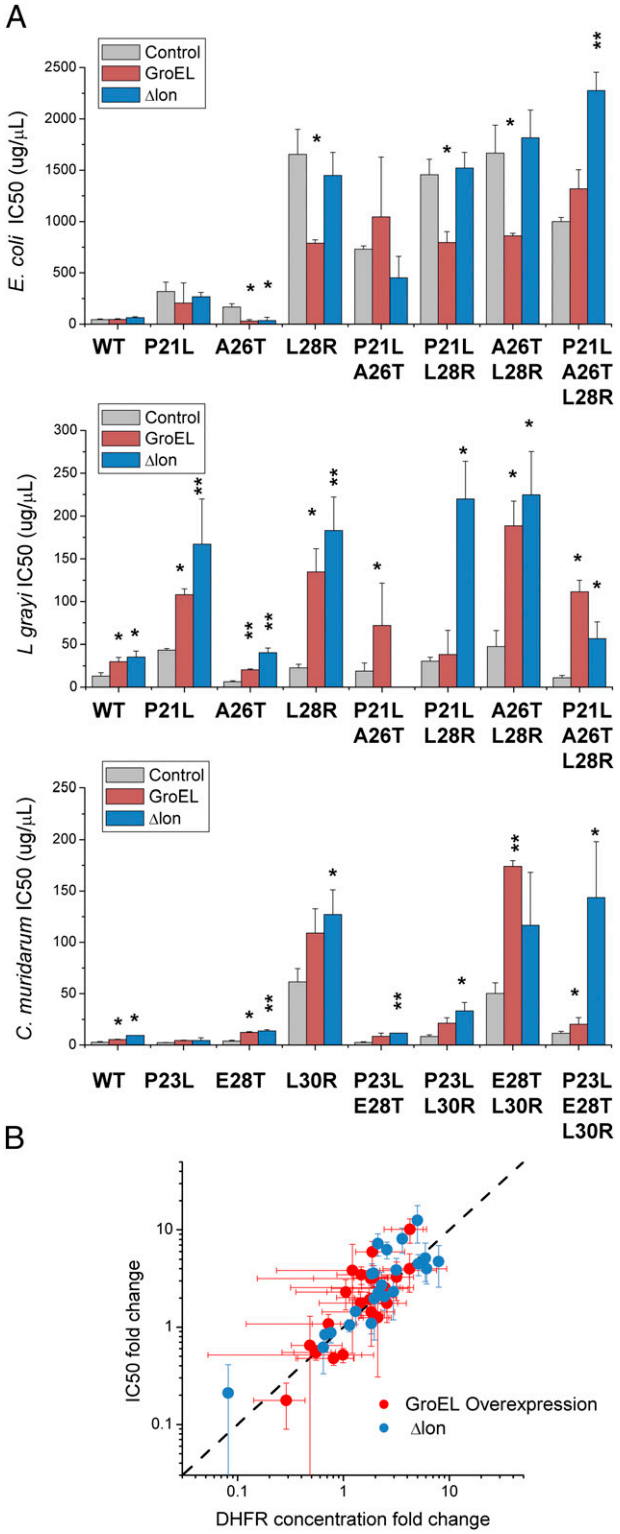

Fig. 4. Resistance to TMP is influenced by components of the PQC system. (*A*) Impact of GroEL overexpression and Lon protease deletion on IC_{50} (mean ± SEM) determined for *E. coli* and orthologous DHFR mutants from *L. grayi* and *C. muridarum*. $*P < 0.05$, $**P < 0.005$. (*B*) Effect of GroEL overexpression and Lon deletion affect IC_{50} mostly through their effect on protein abundance. Protein abundances were determined for various *E. coli*, *L. grayi*, and *C. muridarum* DHFR mutants under GroEL overexpression or Lon deletion. The dotted line shows a theoretical linear dependence with slope = 1.

relationship for DHFR. We showed that a unique combination of molecular parameters can serve as an accurate predictor of fitness from the biophysical properties of the enzyme alone. The resulting biophysical fitness landscape makes it possible to predict fitness across a broad range of concentrations of TMP.

We found that no single molecular trait determines the IC_{50} value of antibiotic resistance. Rather, mutations simultaneously affect several properties of DHFR and there is a trade-off between beneficial effects of mutations that weaken the binding to TMP at the expense of partial loss of catalytic activity, resulting in extensive, predominantly negative, epistasis (Table 1). Furthermore, the analysis presented in Fig. 5 suggests that the relative importance of fitness contributions of different molecular traits varies with conditions such as concentration of antibiotic; strong effect of a drug concentration on the relative fitness of alleles of *Plasmodium vivax* DHFR is a clear example (6). Importantly, relevant molecular properties of target proteins (stability, catalysis, and drug binding) can be determined in a broad range of conditions such as temperature and pH, allowing one to extend the trait-specific landscape predictions into a broader range of environments. The analysis for properties that are governed by biological processes, such as protein abundance, is more challenging because this requires a deeper understanding of complex cellular mechanisms. Activation of DHFR promoter is particularly important because it directly affects the intracellular abundance. The emergence of mutations in the promoter region during TMP adaptation clearly highlights its role in evolution (1); however, many aspects of transcription feedback for DHFR are still poorly understood. Such complexities do not affect the results of our work, because the expression of DHFR here is plasmid-based.

We also found that PQC plays an important role in sculpting the fitness landscape of antibiotic resistance, in some cases determining the genomic outcome of adaptation. For example, both our analysis and ref. 2 indicate that the triple mutant of *E. coli* DHFR has lower IC_{50} than several other mutants, yet it gets fixed at higher concentration of TMP in dynamic morbidostat experiments in ref. 1. The triple mutant becomes a clear winner on the Δ*lon* background. It is, therefore, possible that Lon inactivation or, alternatively, a significant down-regulation of the intracellular Lon levels, may have preceded the fixation of the triple mutant. Indeed, inactivation of Lon via insertion of the mobile element IS186 was observed previously in adaptation to other antibiotics (5, 27) and in adaptation after orthologous replacement of DHFR (20). Furthermore, a dramatic drop in Lon abundance in response to chromosomal integration of destabilized DHFR mutants has been observed (24). Similarly, up-regulation of GroEL can serve as an adaptive mechanism to buffer the deleterious effects of mutations (31, 32), in our case by rescuing molten-globule intermediates. Conversely, we found that GroEL+ can also be deleterious for the mutants with increased stability (L28R in *E. coli*). The mechanism of such deleterious effect remains to be established. Again, a detailed characterization of how Lon, GroEL, and possibly other elements of PQC respond to different factors (e.g., TMP-induced stress) is fundamental to improve the accuracy of fitness landscapes prediction at conditions more similar to those found in several evolutionary experiments.

The Monod-type dependence of fitness on protein activity as presented in Eq. **1** was predicted by Kacser and Burns (14) and found experimentally in the analysis of fitness for the mutant forms of *lac* operon proteins β-permease and β-galactosidase (15). More recently we found that same relation holds for fitness in strains with orthologous DHFR replacements (20). Bolon and coworkers (33) found that a similar Monod "elasticity curve" well describes fitness effects of variation of Hsp90 expression in yeast. It is, therefore, likely that the Monod dependence in Eq. **1** is generally applicable to a broad range of fitness effects, and our analysis could be extended either to different organisms or to the

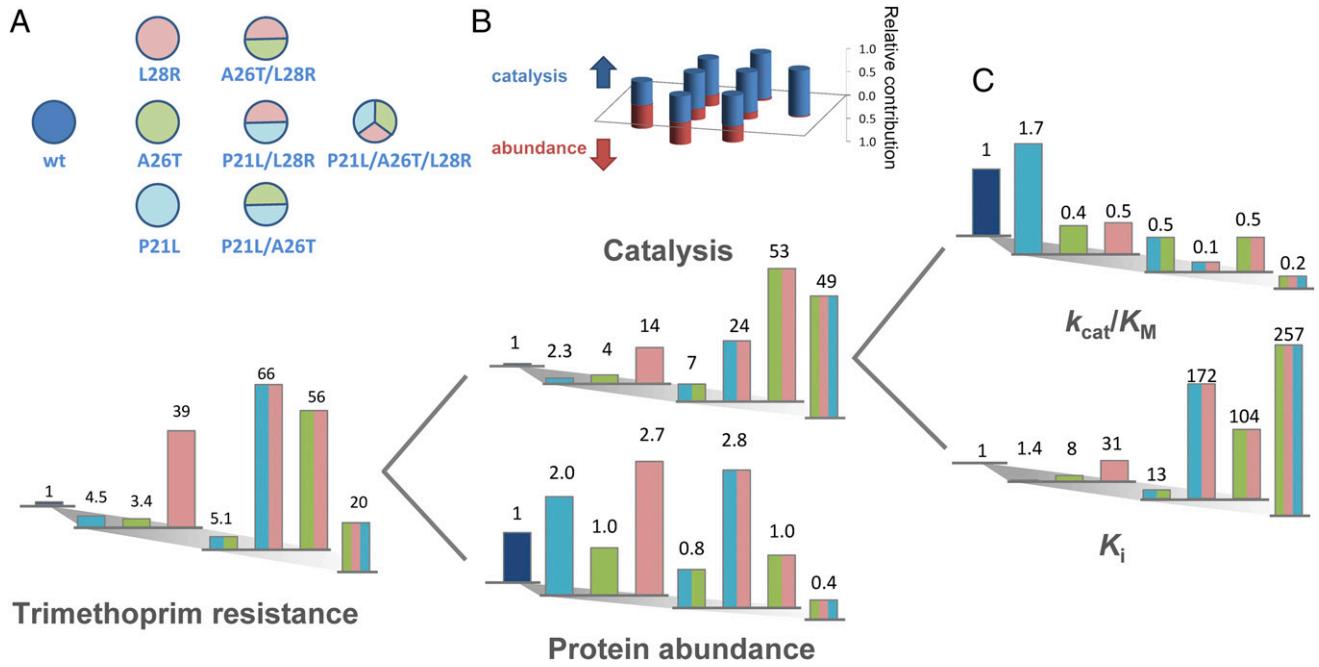

Fig. 5. Quantitative dissection of fitness into multiple microscopic landscapes of different molecular traits. (*A*) Relative resistance to TMP computed by the product $[DHFR] \times k_{cat}/K_m \times K_i$. (*B*) Relative contribution of protein abundance and catalysis to overall fitness. (*C*) Catalysis term is decomposed into catalytic efficiency and K_i.

adaptation against antibiotics that target other enzymes. In any case, it might be expected that under different experimental conditions a Monod-type fit of the curve shown in Fig. 3*A* would result in a different value of the fitted parameter *B*. This variable is a property of the system and pathway-specific and thus should be measured whenever the conditions are different.

The major advantage of biophysical mapping of a fitness landscape is that it can predict fitness not only across a broad range of conditions but also potentially can be used for predicting the fitness effects of de novo mutations. Recent advances in computational methods for predicting the effects of mutations on DHFR stability are definitively valuable (34); however, computational prediction of mutational changes in catalytic properties is still an important bottleneck in this direction. A multiscale approach that merges molecular analysis with biophysical fitness landscapes and population-level evolutionary dynamics would then provide a path to predict in silico and in vitro the outcomes of key adaptation events such as bacterial and viral escape from antibodies and antibiotics.

Methods

DHFR Gene Constructs. All seven possible combinations of mutations at three sites (P21L, A26T, and L28R) of *E.coli folA* gene were introduced by QuickChange Site-Directed Mutagenesis Kit (Stratagene) and cloned into the expression vector pFLAG (Sigma-Aldrich). Each mutagenized plasmid was sequenced to confirm the presence of expected mutations, and the absence of any other mutations. Similarly, we constructed all possible combinations of mutations in the genes coding for DHFR proteins from *C. muridarum* and *L. grayi* in the loci corresponding to the three resistant mutations in *E. coli* DHFR. These sites are P23L, E28T, and L30L for *L. grayi* and P21L, A26T, and L28R for *C. muridarum*.

Growth Measurements and IC_{50} Determination. Cultures grown overnight at 37 °C in M9 minimal medium were normalized to an OD of 0.1 with fresh medium. When appropriate, GroEL overexpression and/or increase in DHFR concentrations were induced by adding arabinose and IPTG immediately after normalization. After additional growth during 5–6 h a new normalization to an OD = 0.1 was performed before inoculation of 96-well plates (1/5 dilution) containing M9 medium and 12 different concentrations of TMP (0–2,500 μg/mL). The plates were incubated at 37 °C with orbital shacking and absorbance measurements at 600 nm were taken every 30 min during 15 h. Growth was quantified by integration of the area under the growth curve (OD vs. time) between 0 and 15 h, as described in ref. 2. Growth integrals determined for a given mutant were normalized in respect to the corresponding growth of that mutant measured in the absence of TMP. IC_{50} values were determined from the fit of a logistic equation to plots of growth vs. TMP concentrations. Reported IC_{50} are averaged from at least three replicates and SEs are indicated.

Measurements of Intracellular Protein Abundance. Cells from cultures grown at 37 °C were lysed with 1× Pop Culture reagent (Merck Millipore) in the presence of 1× complete protease inhibitor mixture (Roche). The lysate was cleared by centrifugation and the soluble fraction was transferred to 96-well white plates for total activity measurements. The lysate was preincubated with 100 μM NADPH and the reaction was started with the addition of 50 μM dihydrofolate. The decrease in fluorescence (excitation at 300 nm and emission at 400 nm) was measured over 20 min at 25 °C. Protein abundance was determined by dividing the total activity by k_{cat}.

Protein Overexpression and Purification. *E. coli* BL21 cells transformed with pFLAG + C-terminal His-tagged DHFR were grown in Terrific broth medium and protein overexpression was induced when OD = 1 with 100 μM IPTG during ∼18 h at 300 rpm and 20 °C. The recombinant proteins were purified from clarified cell lysates on Ni-NTA columns (Qiagen) followed by size-exclusion chromatography separation (Superdex 75 10/300 GL).

Steady-State Kinetic Measurements. DHFR kinetic parameters were measured by progress-curve kinetics, essentially as described before (13). The reaction was carried out in MTEN buffer [50 mM 2-(*N*-morpholino)ethanesulfonic acid, 25 mM Tris(hydroxymethyl)aminomethane, 25 mM ethanolamine, and 100 mM sodium chloride, pH 7] at 25 °C and was monitored spectrophotometrically to follow the decrease in absorbance at 340 nm due to NADPH oxidation. The kinetics parameters (k_{cat} and K_m) were derived from progress-curves analysis using Global Kinetic Explorer (35) by simultaneous fitting of data obtained at two different dihydrofolate concentrations (2.5 and 10 μM).

Determination of Inhibition Constants (K_i) for TMP. Inhibition constants were determined from kinetic competition experiments performed at fixed substrate concentration 100 μM NADPH and 30 μM dihydrofolate and varying inhibitor concentrations. Activity measurements were performed at 25 °C by following NADPH oxidation at 340 nm. Inhibition constants were calculated from plots of activity vs. inhibitor concentration by fitting a competitive-type inhibition equation (36).

Thermal Denaturation. DHFR solutions (5 μM) were prepared in 50 mM phosphate buffer and 1 mM DTT at pH 7.0 in the presence of 100 μM NADPH. A temperature ramp of 1 °C/min was set between 25 and 90 °C, and the fluorescence intensity at 370 and 320 nm was recorded upon excitation at 280 nm. Thermal melting curves were analyzed by plotting the ratio of intensities 370/320 nm.

bis-ANS Fluorescence Measurements. DHFR protein solutions (2 μM) in the presence of 12 μM of bis-ANS were prepared in 50 mM phosphate and 1 mM DTT at pH 7.0 and placed in a 1-cm path-length quartz cuvette. The samples were equilibrated for 5 min at 37 °C and the fluorescence emission spectra between 460 and 600 nm were recorded upon excitation at 395 nm. The emission band was integrated and the background of bis-ANS fluorescence in the absence of protein was subtracted. Intensity integrals were normalized to WT *E. coli.* DHFR.

ACKNOWLEDGMENTS. We thank Roy Kishony for very helpful comments. This work was funded by National Institute of General Medical Sciences Grant GM068670 (to E.I.S.) and NIH Grant AI106734 (to D.L.H.).

1. Toprak E, et al. (2012) Evolutionary paths to antibiotic resistance under dynamically sustained drug selection. *Nat Genet* 44(1):101–105.
2. Palmer AC, et al. (2015) Delayed commitment to evolutionary fate in antibiotic resistance fitness landscapes. *Nat Commun* 6:7385.
3. Lozovsky ER, et al. (2009) Stepwise acquisition of pyrimethamine resistance in the malaria parasite. *Proc Natl Acad Sci USA* 106(29):12025–12030.
4. Weinreich DM, Delaney NF, Depristo MA, Hartl DL (2006) Darwinian evolution can follow only very few mutational paths to fitter proteins. *Science* 312(5770):111–114.
5. Oz T, et al. (2014) Strength of selection pressure is an important parameter contributing to the complexity of antibiotic resistance evolution. *Mol Biol Evol* 31(9): 2387–2401.
6. Jiang PP, Corbett-Detig RB, Hartl DL, Lozovsky ER (2013) Accessible mutational trajectories for the evolution of pyrimethamine resistance in the malaria parasite Plasmodium vivax. *J Mol Evol* 77(3):81–91.
7. Neher RA, Russell CA, Shraiman BI (2014) Predicting evolution from the shape of genealogical trees. *eLife* 3:3.
8. Lobkovsky AE, Wolf YI, Koonin EV (2011) Predictability of evolutionary trajectories in fitness landscapes. *PLOS Comput Biol* 7(12):e1002302.
9. Costanzo M, et al. (2010) The genetic landscape of a cell. *Science* 327(5964):425–431.
10. Ostman B, Hintze A, Adami C (2012) Impact of epistasis and pleiotropy on evolutionary adaptation. *Proc Biol Sci* 279(1727):247–256.
11. Lázár V, et al. (2014) Genome-wide analysis captures the determinants of the antibiotic cross-resistance interaction network. *Nat Commun* 5:4352.
12. Bershtein S, Mu W, Shakhnovich EI (2012) Soluble oligomerization provides a beneficial fitness effect on destabilizing mutations. *Proc Natl Acad Sci USA* 109(13): 4857–4862.
13. Bershtein S, Mu W, Serohijos AW, Zhou J, Shakhnovich EI (2013) Protein quality control acts on folding intermediates to shape the effects of mutations on organismal fitness. *Mol Cell* 49(1):133–144.
14. Kacser H, Burns JA (1981) The molecular basis of dominance. *Genetics* 97(3-4): 639–666.
15. Dykhuizen DE, Dean AM, Hartl DL (1987) Metabolic flux and fitness. *Genetics* 115(1): 25–31.
16. Ptitsyn OB (1995) Molten globule and protein folding. *Adv Protein Chem* 47:83–229.
17. Goldberg ME, et al. (1990) An early immunoreactive folding intermediate of the tryptophan synthease beta 2 subunit is a 'molten globule'. *FEBS Lett* 263(1):51–56.
18. Fierke CA, Johnson KA, Benkovic SJ (1987) Construction and evaluation of the kinetic scheme associated with dihydrofolate reductase from Escherichia coli. *Biochemistry* 26(13):4085–4092.
19. Taniguchi Y, et al. (2010) Quantifying E. coli proteome and transcriptome with single-molecule sensitivity in single cells. *Science* 329(5991):533–538.
20. Bershtein S, et al. (2015) Protein homeostasis imposes a barrier on functional integration of horizontally transferred genes in bacteria. *PLoS Genet* 11(10):e1005612.
21. Bennett BD, et al. (2009) Absolute metabolite concentrations and implied enzyme active site occupancy in Escherichia coli. *Nat Chem Biol* 5(8):593–599.
22. Werner RG, Goeth H (1984) Trimethoprim, failure to penetrate into Pseudomonas-aeruginosa cells. *FEMS Microbiol Lett* 23(2-3):201–204.
23. Bollenbach T, Quan S, Chait R, Kishony R (2009) Nonoptimal microbial response to antibiotics underlies suppressive drug interactions. *Cell* 139(4):707–718.
24. Bershtein S, Choi JM, Bhattacharyya S, Budnik B, Shakhnovich E (2015) Systems-level response to point mutations in a core metabolic enzyme modulates genotype-phenotype relationship. *Cell Reports* 11(4):645–656.
25. Kitagawa M, et al. (2005) Complete set of ORF clones of Escherichia coli ASKA library (a complete set of E. coli K-12 ORF archive): Unique resources for biological research. *DNA Res* 12(5):291–299.
26. Flensburg J, Sköld O (1987) Massive overproduction of dihydrofolate reductase in bacteria as a response to the use of trimethoprim. *Eur J Biochem* 162(3):473–476.
27. Nicoloff H, Andersson DI (2013) Lon protease inactivation, or translocation of the lon gene, potentiate bacterial evolution to antibiotic resistance. *Mol Microbiol* 90(6): 1233–1248.
28. de Visser JA, Krug J (2014) Empirical fitness landscapes and the predictability of evolution. *Nat Rev Genet* 15(7):480–490.
29. Chou HH, Delaney NF, Draghi JA, Marx CJ (2014) Mapping the fitness landscape of gene expression uncovers the cause of antagonism and sign epistasis between adaptive mutations. *PLoS Genet* 10(2):e1004149.
30. Jacquier H, et al. (2013) Capturing the mutational landscape of the beta-lactamase TEM-1. *Proc Natl Acad Sci USA* 110(32):13067–13072.
31. Tokuriki N, Tawfik DS (2009) Chaperonin overexpression promotes genetic variation and enzyme evolution. *Nature* 459(7247):668–673.
32. Queitsch C, Sangster TA, Lindquist S (2002) Hsp90 as a capacitor of phenotypic variation. *Nature* 417(6889):618–624.
33. Jiang L, Mishra P, Hietpas RT, Zeldovich KB, Bolon DN (2013) Latent effects of Hsp90 mutants revealed at reduced expression levels. *PLoS Genet* 9(6):e1003600.
34. Tian J, Woodard JC, Whitney A, Shakhnovich EI (2015) Thermal stabilization of dihydrofolate reductase using monte carlo unfolding simulations and its functional consequences. *PLOS Comput Biol* 11(4):e1004207.
35. Johnson KA, Simpson ZB, Blom T (2009) FitSpace explorer: An algorithm to evaluate multidimensional parameter space in fitting kinetic data. *Anal Biochem* 387(1):30–41.
36. Krohn KA, Link JM (2003) Interpreting enzyme and receptor kinetics: Keeping it simple, but not too simple. *Nucl Med Biol* 30(8):819–826.